Supporting Information

Sensitive Colorimetric Glucose Sensor by Iron-based Nanozymes with Controllable Fe Valence

Wenli Zhao,[#a] Guangpu Zhang,[#b] Yang Du,[c] Shuangqin Chen,[a] You Fu,[c] Fan Xu,[a] Xiangyun Xiao,[a] Wei Jiang,*[b] and Qingmin Ji*[a]

[a] *Herbert Gleiter Institute for Nanoscience, School of Materials Science and Engineering, Nanjing University of Science and Technology, 200 Xiaolingwei, Nanjing, 210094, P. R. China.*

[b] *National Special Superfine Powder Engineering Technology Research Center, Nanjing University of Science and Technology, Nanjing 210094, P. R. China.*

[c] *School of Chemical Engineering, Nanjing University of Science & Technology, 200 Xiaolingwei, Nanjing, 210094, P. R. China.*

*Corresponding authors: jiqingmin@njust.edu.cn; superfine_jw@126.com

Additional Data

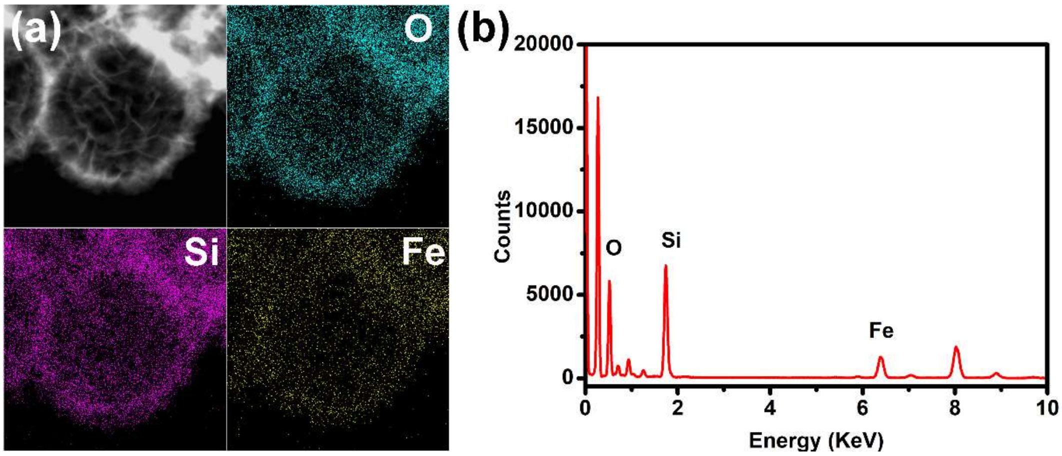

Figure S1. (a) The STEM image and the corresponding element mappings, O (green), Si (red), Fe (yellow) of Fe^{3+}@SHSs; (b) EDS spectroscopy of Fe^{3+}@SHSs

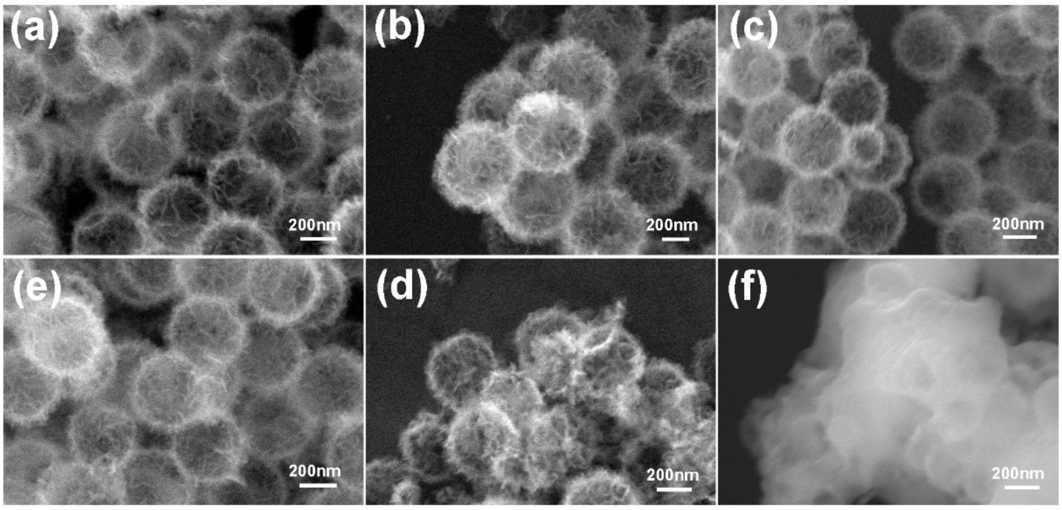

Figure S2. The high-magnification SEM images of (a) Fe^{3+}@SHSs, (b) FeO_x@SHS-300, (c) FeO_x@SHS-400, (d) FeO_x@SHS-500, (e) FeO_x@SHS-600, and (f) FeO_x@SHS-700.

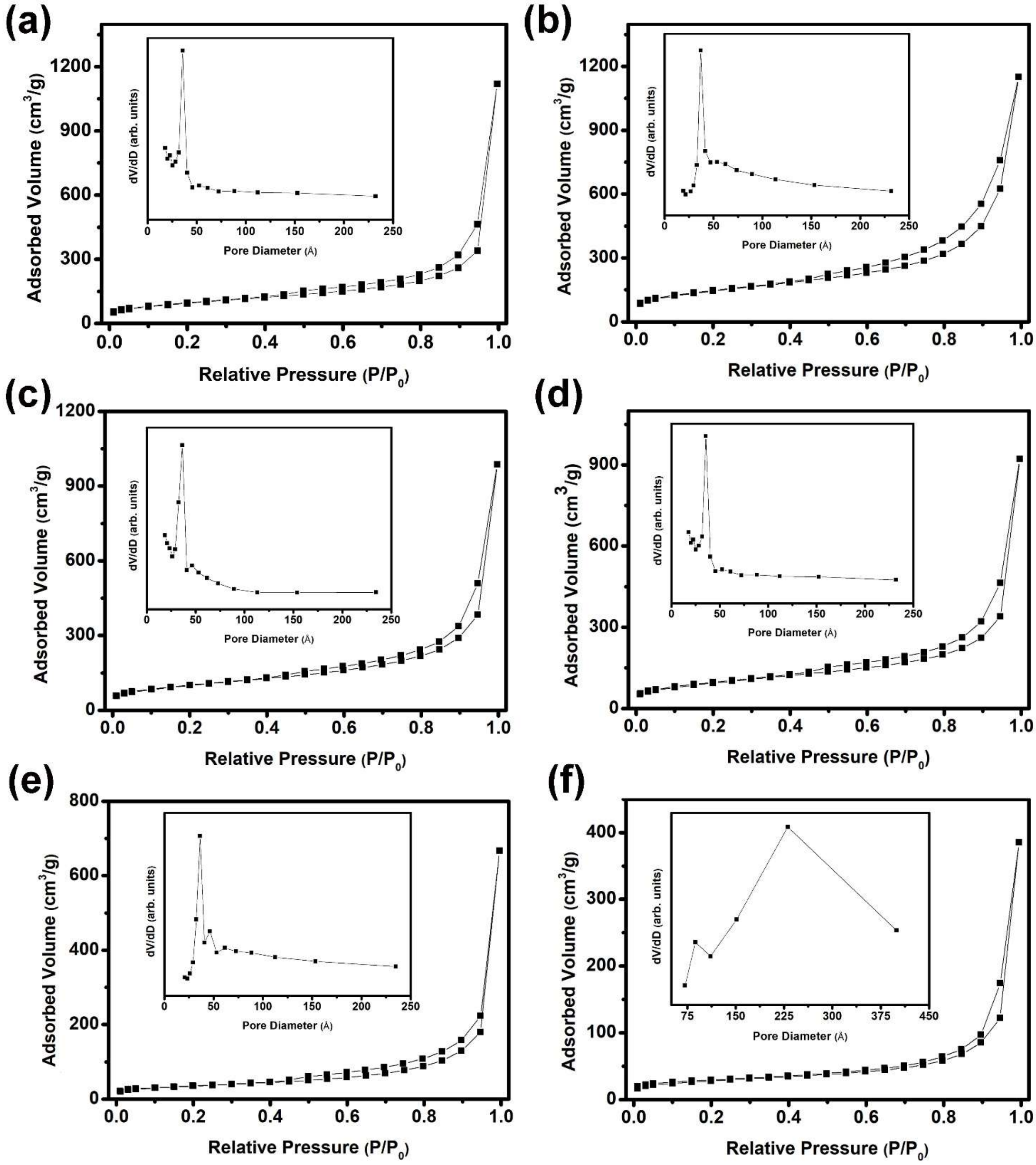

Figure S3. The N_2 adsorption-desorption isotherms and the pore size distribution curves of (a) Fe^{3+}@SHSs; (b) FeO_x@SHS-300; (c) FeO_x@SHS-400; (d) FeO_x@SHS-500; (e) FeO_x@SHS-600; (f) FeO_x@SHS-700.

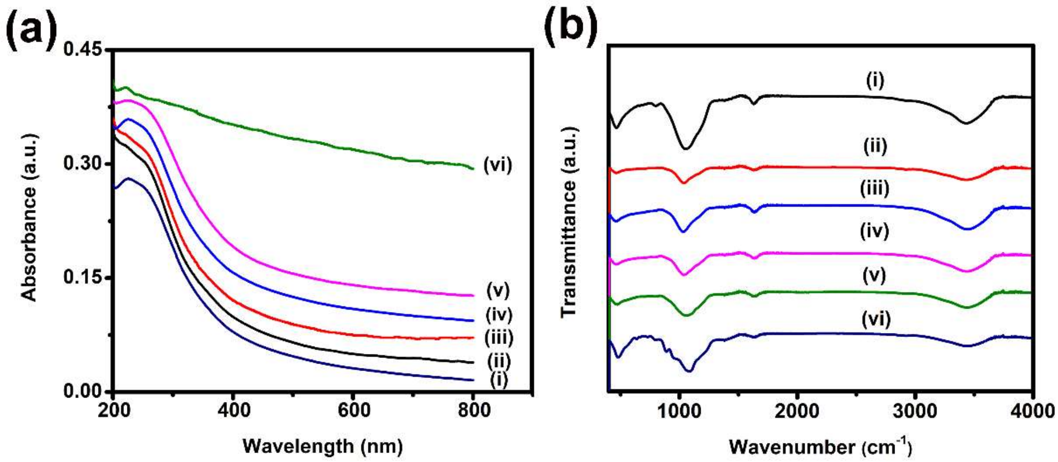

Figure S4. (a) The UV-Vis spectra and (b) the FT-IR spectra of the Fe-doped silica hollow spheres. (i) Fe^{3+}@SHSs; (ii) FeO_x@SHS-300; (iii) FeO_x@SHS-400; (iv) FeO_x@SHS-500; (v) FeO_x@SHS-600 and (vi) FeO_x@SHS-700.

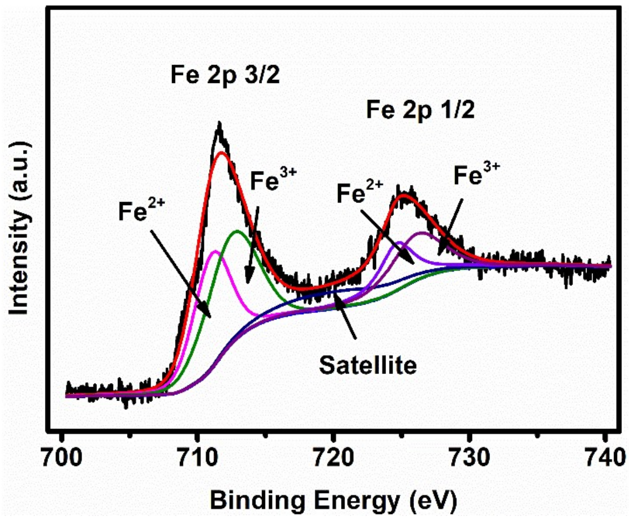

Figure S5. The XPS spectrum of Fe^{3+}@SHSs (before reduction treatment).

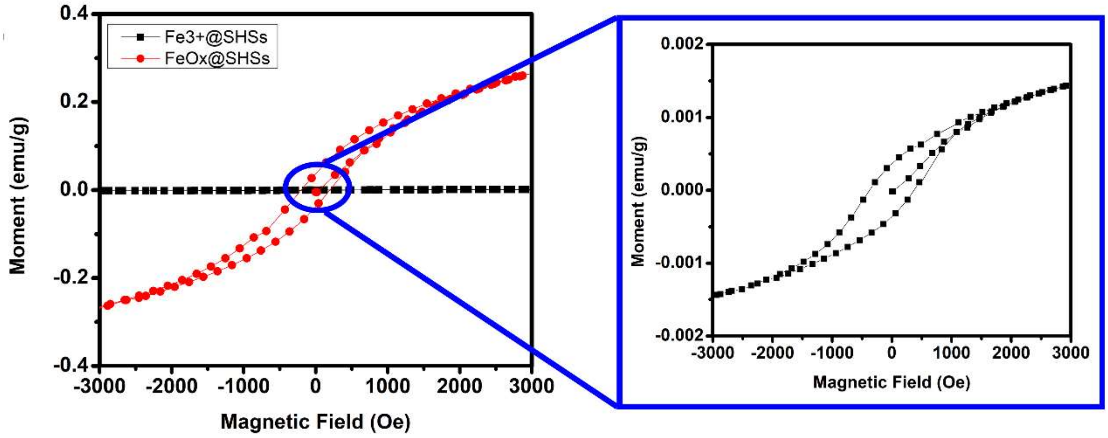

Figure S6. Magnetic hysteresis loops (at 300 K) of the Fe^{3+}@SHSs (before reduction treatment) and FeO_x@SHS-500 (after reduction treatment).

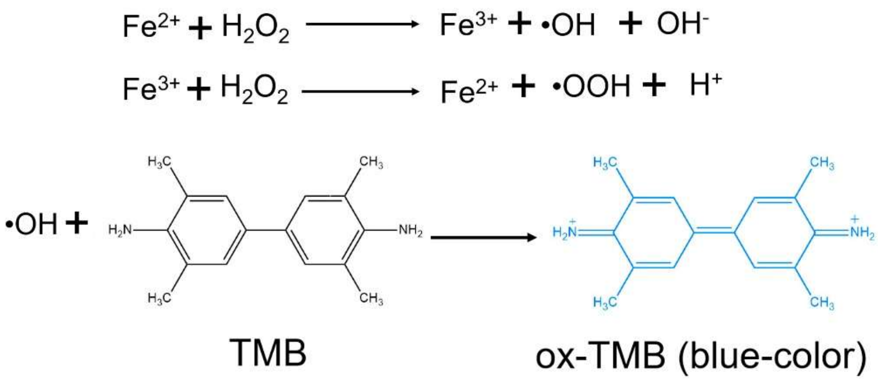

Figure S7. The colorimetric catalytic mechanism of Fe-based nanozyme based on the Fenton reactions.

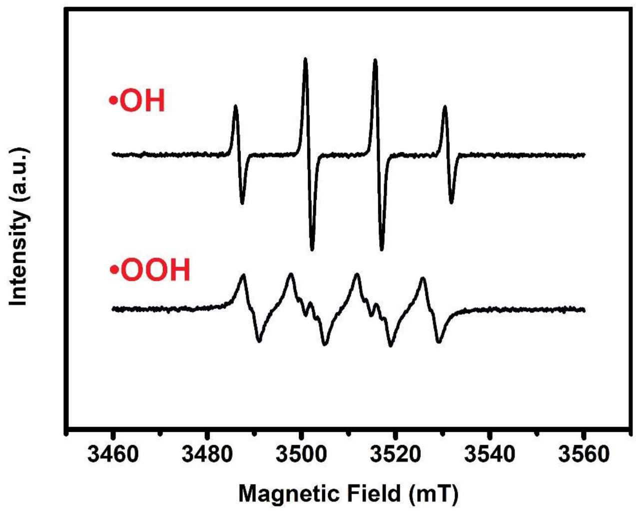

Figure S8. The EPR spin-trap spectra for the reactive oxidative species generated from FeO_x@SHSs in the Fenton process after 5 minutes reacting.

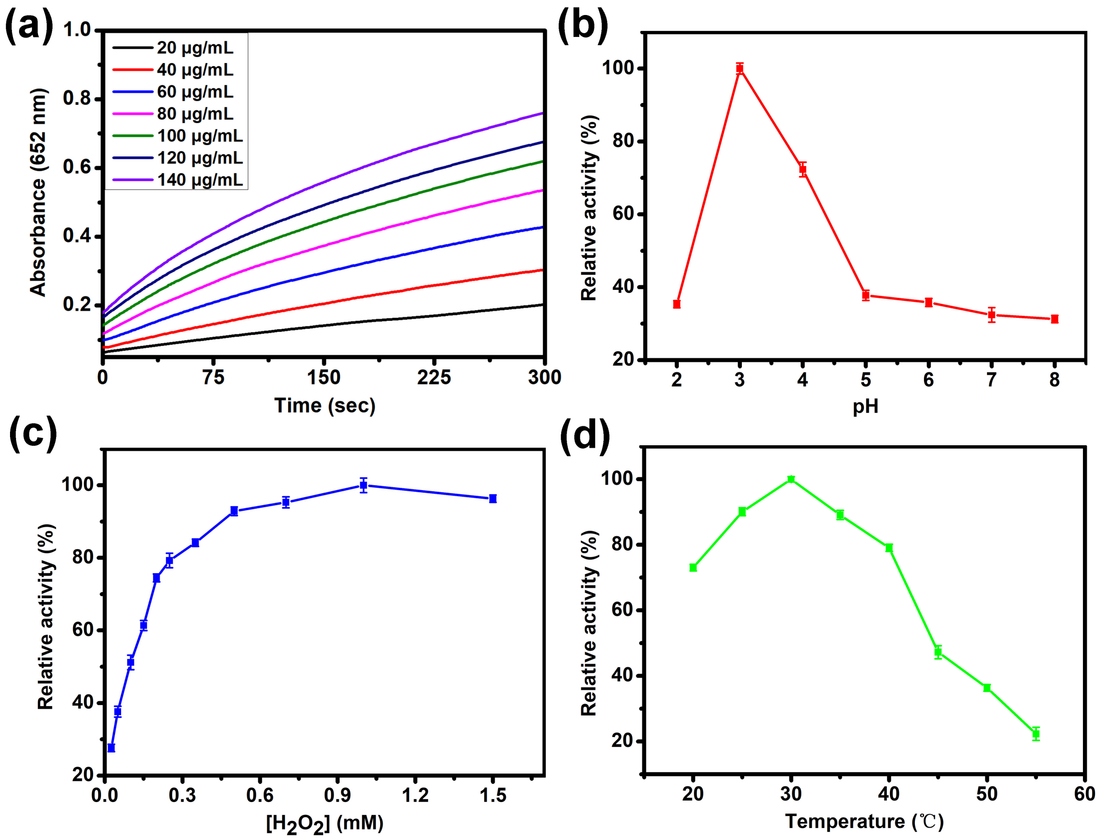

Figure S9. The influence of reaction conditions on the peroxidase-like activity of FeO_x@SHS-500. (a) the amount of catalyst, (b) pH, (c) H_2O_2 concentration, and (d) temperature. The standard error bars were derived from three repeated measurements.

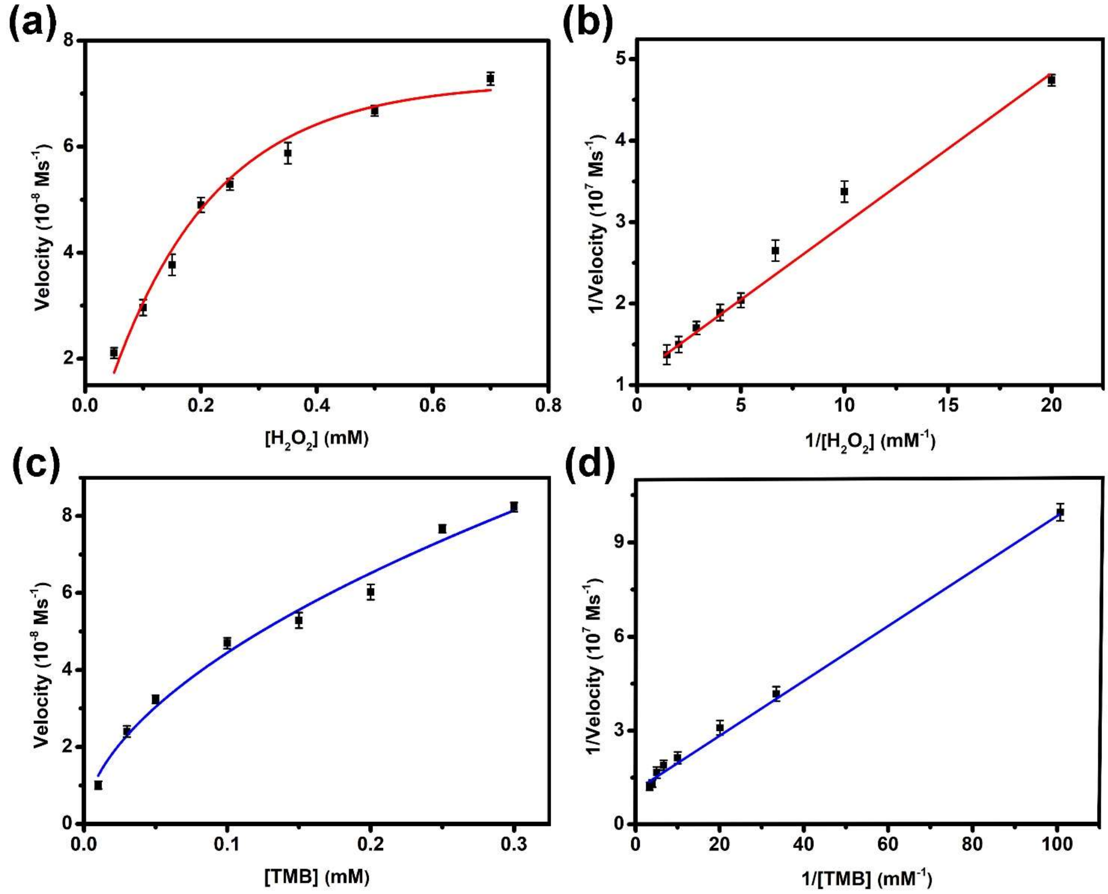

Figure S10. The steady state kinetic analysis for FeO_x@SHS-500 under various conditions. (a) [TMB] = 0.3 mM; [H_2O_2]=0.025-0.7mM, (c) [H_2O_2]=1.0mM; [TMB] = 0.01-0.3 mM; (b) and (d) are the Lineweaver-Burk double reciprocal plots corresponding to conditions (a) and (c). The reaction was carried out with 60 μg/mL catalyst of 0.1 M acetate buffer, pH=3 and temperature=30 °C. The standard error bars were derived from three repeated measurements.

Table S1. The porous parameters of FeO_x@SHSs.

Samples	Calcination temperature	S_{BET} ($m^2\ g^{-1}$)	V ($cm^3 g^{-1}$)
Fe^{3+}@SHSs	-	471.96	0.890
FeO_x@SHS-300	300°C	370.12	0.818
FeO_x@SHS-400	400°C	352.74	0.772
FeO_x@SHS-500	500°C	337.00	0.688
FeO_x@SHS-600	600°C	122.53	0.349
FeO_x@SHS-700	700°C	67.64	1.060

Table S2. Comparison of the catalysis kinetic parameters of various Fe-based nanozymes.

Nanozyme	K_m (mM)		V_{max} (10^{-8} M·S^{-1})		Ref.
	TMB	H_2O_2	TMB	H_2O_2	
HRP	0.434	3.7	10.0	8.71	1
Go-Fe_3O_4	0.43	0.71	13.08	5.31	2
Casein-Fe_3O_4	0.021	4.75	10.6	15.9	3
Fe_3O_4@C	0.313	0.414	19.8	5.25	4
Fe_3O_4@C YSNs	0.27	0.035	12.0	3.34	5
Fe-MSN	0.407	0.01	7.60	4.33	6
$Fe_{0.5}Co_{0.5}$ NPs	1.79	0.06	45.6	13.2	7
Fe_3O_4-MMT	0.025	0.811	9.409	5.139	8
Mesoporous g-Fe_2O_3	0.0997	144.30	52.0	1.84	9
FeNPs@Co_3O_4 HNCs	0.488	0.019	20.6	1.7	10
3D GN with Fe_3O_4 NPs	0.103	1.39	11.6	10.1	11
Fe3O4/N-GQDs	0.19	1.02	13.8	2.76	12
Fe-MOF	2.6	1.3	5.6	2.5	13
GOx@HP-MIL-88B-BA	0.22	0.38	6.8	7.2	14
Fe-rGO sheets	0.071	30	44.6	26.6	15
Co_3O_4@Co-Fe oxide DSNCs	0.48	0.24	5.32	5.18	16
2Fe_2O_3/30Pt/CNTs	0.17	0.053	18.1	6.79	17
MoS2-MIL-101(Fe)	2.279	0.008	22.23	1.212	18
Fe-MIL-88NH_2	0.284	2.06	10.47	7.04	19
FeO_x@SHSs-0.05	0.076	0.154	8.590	8.312	This work

Table S3. Comparison of the detection limit (LOD) of H_2O_2 and glucose using different Fe-based nanozymes.

Nanozyme	H_2O_2		Glucose		Ref.
	linear detection range (μM)	detection limit (μM)	linear detection range (μM)	detection limit (μM)	
Go-Fe_3O_4	1–50	0.32	2–200	0.74	2
Casein-Fe_3O_4	0.5–200	0.20	3–1000	1.00	3
Fe_3O_4@C	0.2–100	0.08	6–100	2.00	4
Fe3O4@C YSNs	1–20	0.39	1–10	1.12	5
Fe-MSN	7.2–100	1.20	4.1–100	1.20	6
$Fe_{0.5}Co_{0.5}$ NPs	/	/	0.5–10	0.01	7
Fe_3O_4-MMT	50–200	5.10	50–200	5.10	8
Mesoporous g-Fe_2O_3	/	/	1–1000	0.90	9
FeNPs@Co_3O_4 HNCs	0.1–30	0.01	0.5–30	0.05	10
3D GN with Fe_3O_4 NPs	/	/	5–500	0.80	11
Fe@PCN-224	2–100	1.60	30–800	22	[20]
Fe-MOF-GOx	/	/	1–500	0.487	13
GOx@HP-MIL-88B-BA	/	/	2–100	0.98	14
Co_3O_4@Co-Fe	0.02–600	0.02	/	/	16
2Fe_2O_3/30Pt/CNTs	/	/	5–20	0.92	17
MoS2-MIL-101(Fe)	0.01–20	0.01	0.01–15	0.01	18
Fe-MIL-88NH2	0.2–200	/	2–300	0.48	19
FeOx@SHSs-500	25–200	0.41	5–600	0.24	This work

References for Supporting

1. L. Gao, J. Zhuang, L. Nie, J. Zhang, Y. Zhang, N. Gu, T. Wang, J. Feng, D. Yang and S. J. N. n. Perrett, 2007, **2**, 577-583.
2. Y.-l. Dong, H.-g. Zhang, Z. U. Rahman, L. Su, X.-j. Chen, J. Hu and X.-g. Chen, *Nanoscale*, 2012, **4**, 3969-3976.
3. Y. Liu, M. Yuan, L. Qiao and R. Guo, *Biosensors Bioelectronics*, 2014, **52**, 391-396.
4. Q. Li, G. Tang, X. Xiong, Y. Cao, L. Chen, F. Xu and H. Tan, *Sensors Actuators B: Chemical*, 2015, **215**, 86-92.
5. N. Lu, M. Zhang, L. Ding, J. Zheng, C. Zeng, Y. Wen, G. Liu, A. Aldalbahi, J. Shi and S. Song, *Nanoscale*, 2017, **9**, 4508-4515.
6. M. Aghayan, A. Mahmoudi, M. R. Sazegar, N. G. Hajiagha and K. Nazari, *New Journal of Chemistry*, 2018, **42**, 16060-16068.
7. Y. Chen, H. Cao, W. Shi, H. Liu and Y. Huang, *Chemical Communications*, 2013, **49**, 5013-5015.
8. K. Wu, X. Zhao, M. Chen, H. Zhang, Z. Liu, X. Zhang, X. Zhu and Q. Liu, *New Journal of Chemistry*, 2018, **42**, 9578-9587.
9. M. K. Masud, J. Kim, M. M. Billah, K. Wood, M. J. Shiddiky, N.-T. Nguyen, R. K. Parsapur, Y. V. Kaneti, A. A. Alshehri and Y. G. Alghamidi, *Journal of Materials Chemistry B*, 2019, **7**, 5412-5422.
10. J. Zhao, W. Dong, X. Zhang, H. Chai and Y. Huang, *Sensors Actuators B: Chemical*, 2018, **263**, 575-584.

11. Q. Wang, X. Zhang, L. Huang, Z. Zhang and S. Dong, *ACS applied materials interfaces*, 2017, **9**, 7465-7471.

12. B. Shi, Y. Su, L. Zhang, M. Huang, X. Li and S. Zhao, *Nanoscale*, 2016, **8**, 10814-10822.

13. W. Xu, L. Jiao, H. Yan, Y. Wu, L. Chen, W. Gu, D. Du, Y. Lin and C. Zhu, *ACS applied materials interfaces*, 2019, **11**, 22096-22101.

14. Z. Zhao, Y. Huang, W. Liu, F. Ye and S. Zhao, *ACS Sustainable Chemistry Engineering*, 2020, **8**, 4481-4488.

15. M. S. Kim, J. Lee, H. S. Kim, A. Cho, K. H. Shim, T. N. Le, S. S. A. An, J. W. Han, M. I. Kim and J. Lee, *Advanced Functional Materials*, 2020, **30**, 1905410.

16. Q. Chen, X. Zhang, S. Li, J. Tan, C. Xu and Y. Huang, *Chemical Engineering Journal*, 2020, 125130.

17. Y. Chen, Q. Yuchi, T. Li, G. Yang, J. Miao, C. Huang, J. Liu, A. Li, Y. Qin and L. Zhang, *Sensors Actuators B: Chemical*, 2020, **305**, 127436.

18. W. Dong, G. Chen, X. Hu, X. Zhang, W. Shi and Z. Fu, *Sensors Actuators B: Chemical*, 2020, **305**, 127530.

19. Y. L. Liu, X. J. Zhao, X. X. Yang and Y. F. Li, *Analyst*, 2013, **138**, 4526-4531.

20. T. Li, P. Hu, J. Li, P. Huang, W. Tong and C. Gao, *Colloids Surfaces A: Physicochemical Engineering Aspects*, 2019, **577**, 456-463.